International Symposium on New Developments in Advanced High-Strength Sheet Steels
19–22 June 2023, Vail, Colo., USA
DOI: 10.33313/298/030

Deformation-Induced Martensitic Transformation at Tensile and Compressive Deformations of High-Carbon Bainitic Steel

Rintaro Ueji[1*], Wu Gong[2], Stefanus Harjo[2], Takuro Kawasaki[2],
Akinobu Shibata[1], Yuuji Kimura[1], Tadanobu Inoue[1], Noriyuki Tsuchida[3]

1 National Institute for Materials Science, 1-2-1 Sengen, Tsukuba, Ibaraki 305-0047, Japan
2 J-PARC center, 2-4 Shirakata, Tokai-mura, Naka-gun, Ibaraki, 319-1195, Japan
3 University of Hyogo, 2167 Shosha, Himeji, Hyogo, 671-2280, Japan
*Email: UEJI.Rintaro@nims.go.jp

Keywords: high carbon steel, bainite, retained austenite, deformation-induced martensitic transformation, tension, compression, in-situ neutron diffraction, elastic anisotropy, texture

INTRODUCTION

Transformation induced plasticity (TRIP) aided steel [1, 2] is one of the advanced high strengthened steels with preferable ductility. The TRIP aided steel includes retained austenite (γ) with bainitic ferrite or partially evolved martensite. At the retained austenite, the deformation-induced martensitic transformation in which austenite transforms to hard martensite by deformation as schematically shown in **Fig.1**(a), occurs and supports large work hardening rate which is preferable to prevent the plastic instability. There are many reports about the TRIP aided steels with various carbon contents. The published data about the tensile strength of the steels with different carbon content are summarized in Fig.1(b) [3-19]. This figure indicates rough tendency that the TRIP aided steel with higher carbon content is useful to obtain the higher tensile strength. Thus, the high-carbon TRIP aided steel is one of the popular topics in the structural materials science.

For the optimization of mechanical properties, the effect of deformation mode, such as tension or compression, on the deformation-induced martensitic transformation should be studied adequately, because it is usual that the mixture of both

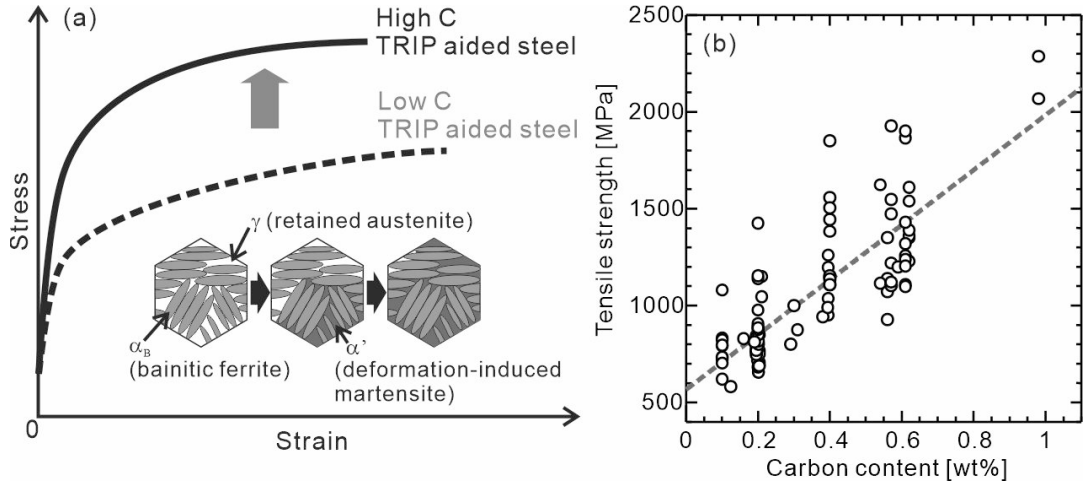

Figure 1. (a) Schematic illustration of stress - strain curve and microstructural change of TRIP aided steels and (b) the tensile strength of low alloyed TRIP aided steels with various carbon contents found in the previous papers.

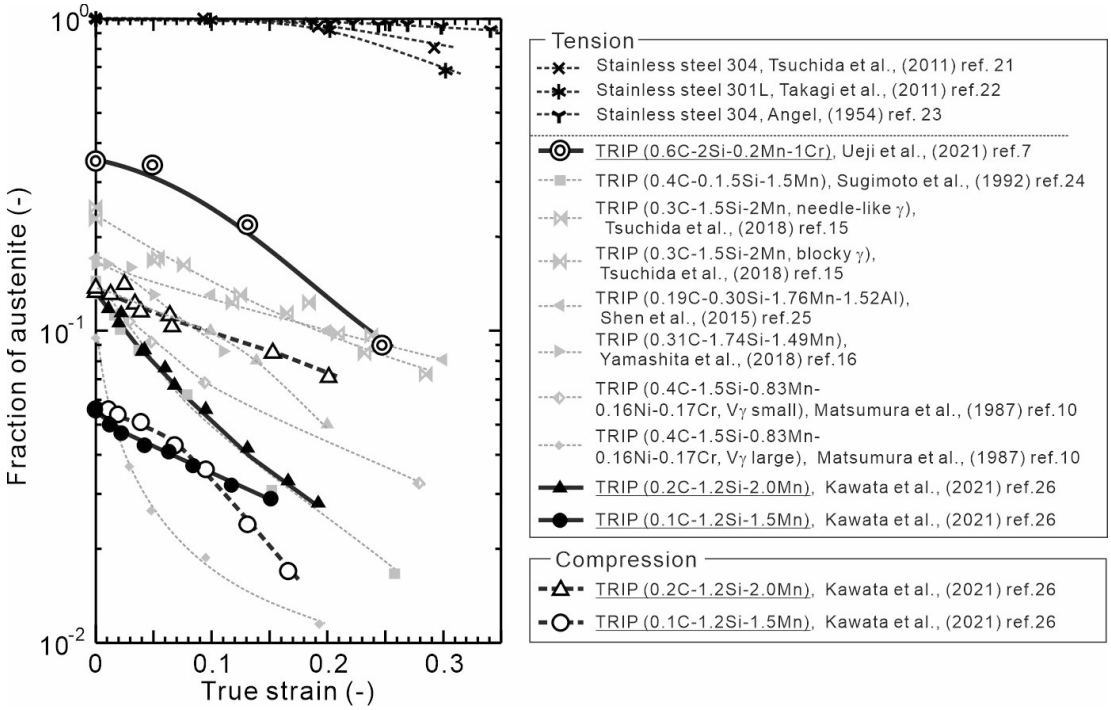

Figure 2. Fraction of austenite at the deformation of various austenitic stainless steels and low-alloyed TRIP aided steels.

tension and compression appears during the forming process of the sheet steel, for example, at bending. The recent studies [3,20] clarified that the deformation-induced martensitic transformation has a strong dependence on the crystallographic orientation parallel to the loading axis . Although this finding seems to give new direction for the texture design of the high-carbon TRIP aided steel, the stress condition in each austenite grains of the TRIP aided steel polycrystals has not been clarified adequately. **Figure 2** shows the previously published data of the volume fraction of austenite in the various steels [7,10,15,16,21-26]. These data were plotted as a function of strain applied at room temperature. Most of the data were examined by tensile deformation, while available data for the compression test are limited, except for the paper by Kawata et al.[26] Consequently, the aim of this paper is to clarify the kinetics of the deformation-induced martensitic transformation in the high carbon TRIP aided steel both at tension and at compression.

EXPERIMENTAL PROCEDURES

A carbon steel (0.62%C-2.02%Si-0.23%Mn-1.01%Cr-Fe) whose chemical composition was designed based on a spring steel with the additional bearing of Si to prevent from the carbide precipitation was examined. The Time-Temperature-Transformation (TTT) diagram of this steel has been reported in the previous paper [7]. Based on the TTT diagram, the austempering condition was determined as a bainitic transformation temperature of 400 °C. The samples with a dimension of 14 mm x 14 mm x 150 mm were austenitized at 850 °C for 600 sec, and then soaked in a salt bath at 400 °C for 1800 sec to obtain fully bainitic structure with retained austenite. The heat-treated samples were cut to the tensile test pieces. The conventional tensile test was conducted with a test piece having a gage length of 42 mm and a diameter of 6 mm, and tested at room temperature at a constant cross head speed of 0.85 mm/min (an initial strain rate of 0.33 x 10^{-4}/sec). The compression test with a cylindrical sample with a height of 12 mm and a diameter of 8 mm was conducted at room temperature at a constant strain rate of 10^{-4}/s.

One tensile test and one compressive test at room temperature were conducted with a high resolution and high intensity time-of-fright (TOF) neutron diffractometer (TAKUMI) at the Beam Line No.19 in Japan Proton Accelerator Research Complex (J-PARC) center. At TAKUMI, a sample at tensile or compressive deformation is able to be examined as the diffraction vector is parallel to the loading axis as shown in **Fig.3**. The tensile test piece has a dimension with a gage length of 40 mm and a diameter of 6 mm and the compressive test piece with a height of 12 mm and a diameter of 5.5 mm was examined. These test pieces were deformed at a quasi-static strain rate, and the diffraction patterns were repeatedly measured at the initial and the loaded states. Data analyses were performed with using a Rietveld software called Z-Rietveld [27]. Due to the arrangement of diffraction

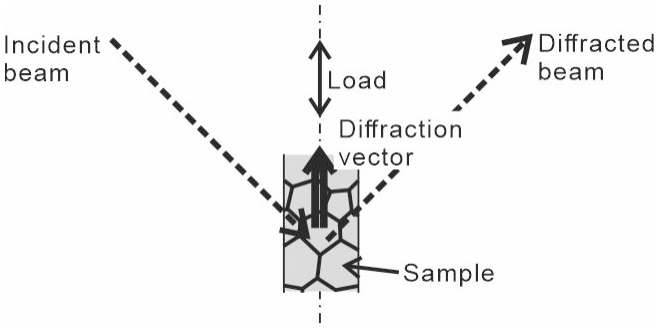

Figure 3. Geometry of in situ diffraction measurement during loading.

measurement system, the spacing of the {*hkl*} plane of the grains in which <*hkl*> direction was parallel to the loading axis, was evaluated with the *hkl* diffraction peak. Thus, lattice strain, $\varepsilon_{hkl}$was evaluated with the following equation (1):

$$\varepsilon_{hkl} = (d_{hkl} - d^0_{hkl}) / d^0_{hkl} \quad (1)$$

where d_{hkl} is {*hkl*} plane spacing obtained from the diffraction patterns during deformation and d^0_{hkl} is the reference spacing of the as-heat treated sample without any loading [28].

Microstructures were examined by an optical microscope and a scanning electron microscope (SEM) with an electron back scattering diffraction (EBSD) measurement system. The optical microscopy was conducted with an 3 % nital etching. The observation surface for SEM was prepared by mechanical gliding and electro-chemical polishing with a solution of 10 vol% perchloric acid + 90 vol% acetic acid at an applied voltage of about 30 V for a polishing time of 1 min at room temperature. SEM (JEOL 7000F) observation was conducted at an accelerated voltage of 15 kV and EBSD measurements (TSL OIM Data Collection） were done at a scanning pitch of 0.2 μm. BCC and FCC phases were set as the possible phases.

RESULTS AND DISCUSSION

Microstructure and stress - strain curves of the 0.6%C bainitic steel

Figure 4 shows the microstructure of the as-heat treated sample of the 0.6%C bainitic steel. Optical microstructure (a) reveals typical morphology of bainite without any large proeutectoid ferrite or pearlite. The crystallographic orientations obtained by the EBSD measurement were illustrated by gray-scale map indicating the orientation perpendicular to the scanned plane with the gray-scale code in the standard triangle at the top-right of this figure. Although the martensite has BCT structure precisely, it is difficult for the conventional EBSD measurement to distinguish the c-axis due to small c/a ratio. Thus, the diffraction data were analyzed with the assumption that all phases can be indexed as BCC or FCC. The orientations of the FCC (b) and BCC (c) at the same measured area were displayed separately. The dotted line of the orientation maps shows the prior austenite grain boundary (PAGB). The area fraction of retained austenite was 35 %. The FCC map shows the area at which the orientations of the retained austenite particles are almost the same. This indicated that the prior austenite grain size, d_γ, was 16 μm. The BCC map (c) shows the elongated bainitic ferrite. This morphology was the same as that reported by the authors previously [3,7]. According to these previous works, the carbon content of the retained austenite was ranging from 1.0 wt% to 1.4 wt%. This content was similar to that in the low caron TRIP aided steels as reported by Sugimoto et al.[29]

Figure 5 shows the true stress - true strain curves at the tension or compression of the 0.6%C bainitic steel. The tensile test showed very little local elongation (necking) even after the fracture. At the compression test, no significant bulging was detected even at the sample deformed to a reduction in height of 20%, probably due to preferable lubrication. The true stress and the true strain were evaluated with the assumption that the deformation occurs uniformly and the volume of the deformation part of the specimen keeps constant. The true stress - strain curves show high yield strength (~900MPa) with large uniform strain without any stress dropping. This result indicates that the high carbon TRIP aided steel has preferable mechanical properties as mentioned at the introduction with Fig.1. Although the yield stress at the tension and that at the compression show little difference, the large work hardening found at the tension did not appear at the compression. This difference indicates the

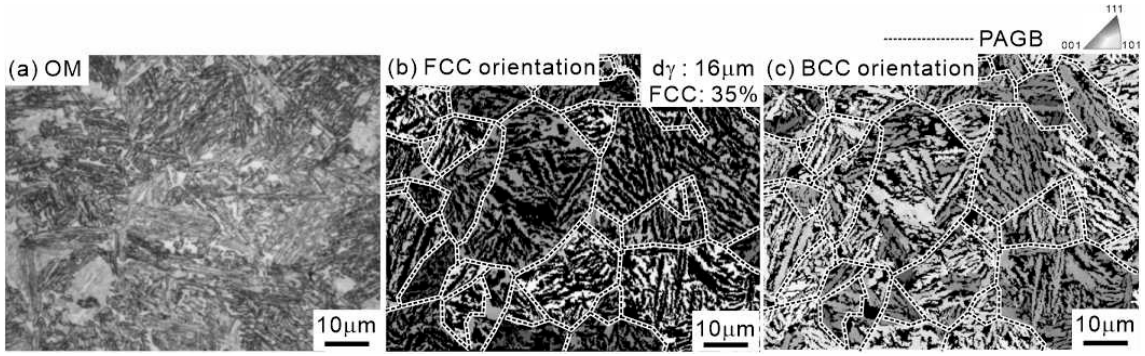

Figure 4. Optical microstructure (a) and the orientation gray-scale maps of the FCC (b) or the BCC (C) phases. The gray-scale indicates the orientation parallel to the normal direction of the measurement plane with the coloring triangle at the right-top of this figure. Dotted line indicates the prior austenite grain boundary (PAGB).

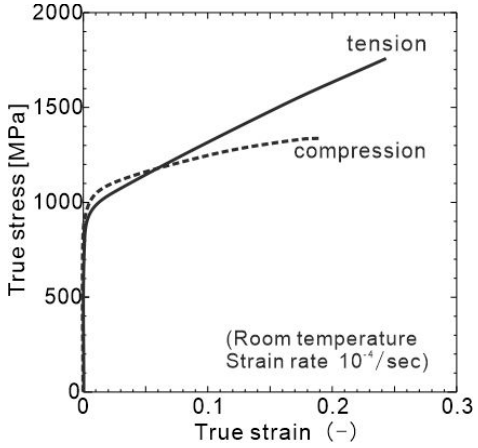

Figure 5. Stress - strain curves of the 0.6%C bainitic steel at the tension or at the compression.

dependence of the stress polarity on the deformation induced martensitic transformation since it is said that the work hardening at the TRIP aided steel was due to the deformation-induced martensitic transformation. In other words, the martensitic transformation in the retained austenite appeared significantly suppressed at the compression.

Lattice strain

According to the previous works [30], the suppression of the martensitic transformation at the compression was explained by the interaction between the applied stress and the expansion accompanied with the martensitic transformation. This interaction can be evaluated only when the precise stress condition is known. However, the spatial distribution of stress in the polycrystalline materials is different from that of single crystal, mainly because of stress dispersion to the different grains of different phases. This can be clarified via the lattice strain measured by in situ neutron diffraction where the lattice strain of the grain with different orientations and different phases can be evaluated [31].

Figure 6 shows the change of lattice strain of the BCC (α) and FCC (γ) phases at the tension (a) and the compression (b). It should be notable that the absolute values of lattice strain and stress were presented even at the compression (b). The diffraction peaks were indexed by BCC or FCC phases as the EBSD measurements were done. The stress - strain curves were displayed as well, and these indicate the macroscopic yield stress (~900MPa). The lattice strain increases linearly at the applied stress lower than the yield stress. These liner slopes are regarded as the diffraction Young's modulus, which are dependent especially on the effective elastic modulus, E_{hkl} which is estimated by the following equation (2):

$$E_{hkl} = \left\{ s_{11} + (2s_{12} - 2s_{11} + s_{44}) \frac{k^2l^2 + l^2h^2 + h^2k^2}{(h^2 + k^2 + l^2)^2} \right\}^{-1} \quad (2)$$

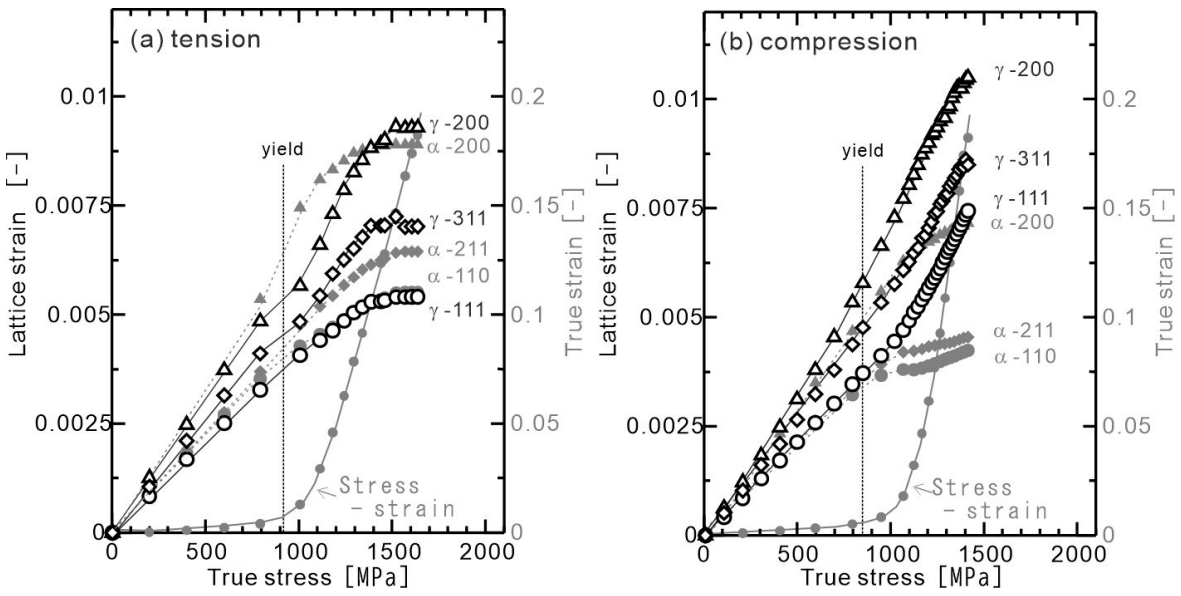

Figure 6. Lattice strain of the 0.6%C bainitic steel at tension (a) or compression (b). Miller indices indicate the corresponding crystallographic planes whose diffraction peaks were evaluated to obtain the lattice strain.

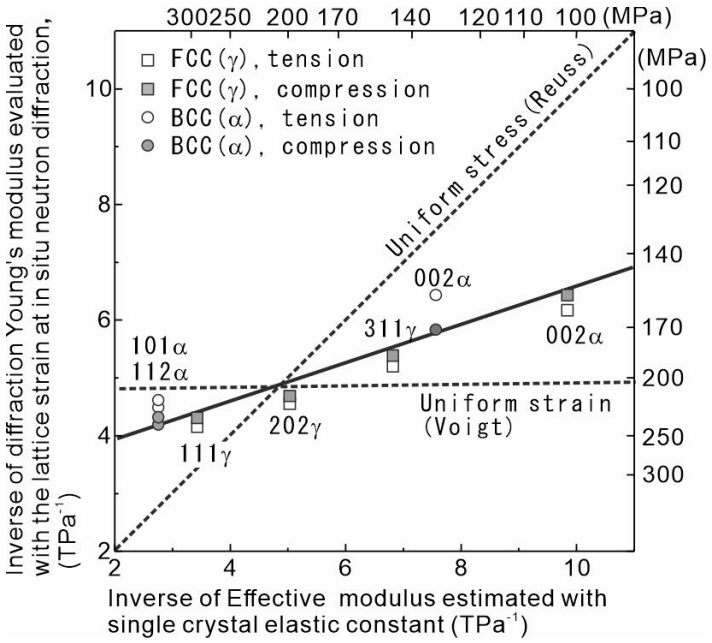

Figure 7. Inverse of the diffraction Young's modulus evaluated with the lattice strain as a function of the inverse of effective modulus evaluated with single crystal elastic constant.

where s_{11}, s_{12} and s_{44} are the elastic compliances [32]. The effective elastic modulus is regarded as Young's modulus of the single crystal at the loading parallel to a given [*hkl*] direction. **Figure 7** shows the inverse of the diffraction Young's modulus as a function of ${E_{hkl}}^{-1}$. When the studied sample can be regarded as a composite material with different components with different Young's modulus, the dispersion of applied stress (elastic strain) to the components can be expressed by the uniform stress model (Reuss model) or the uniform strain model (Voigt model). The estimated diffraction Young's modulus by these two models were illustrated by dotted lines in Fig.7. This work clearly shows that the deformation dispersion in the 0.6%C bainitic steel both at the tension and at the compression follows the average value between those estimated by the Voigt and the Reuss models. This result is well consistent with the previous study on the tensile deformation of the duplex steel by in-situ neutron diffraction [31]. The loading orientation dependence on the stress dispersion can be explained merely by the effective elastic modulus, both at the tension and at the compression.

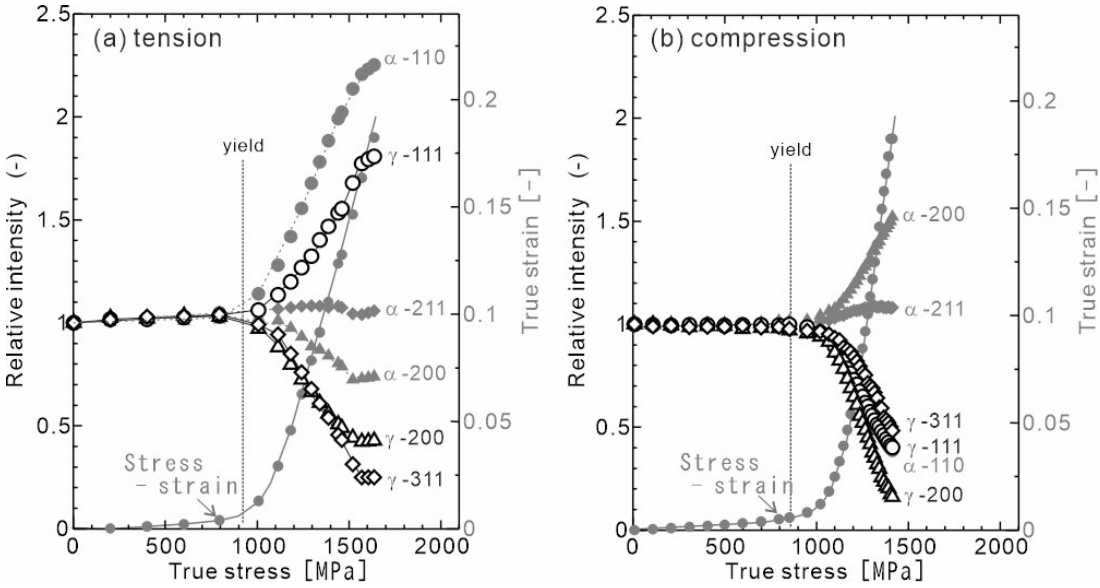

Figure 8. Relative intensity of the in-situ diffraction peaks of the 0.6%C bainitic steel at tension (a) or compression (b). Miller indices indicate the corresponding crystallographic planes whose diffraction peaks were evaluated.

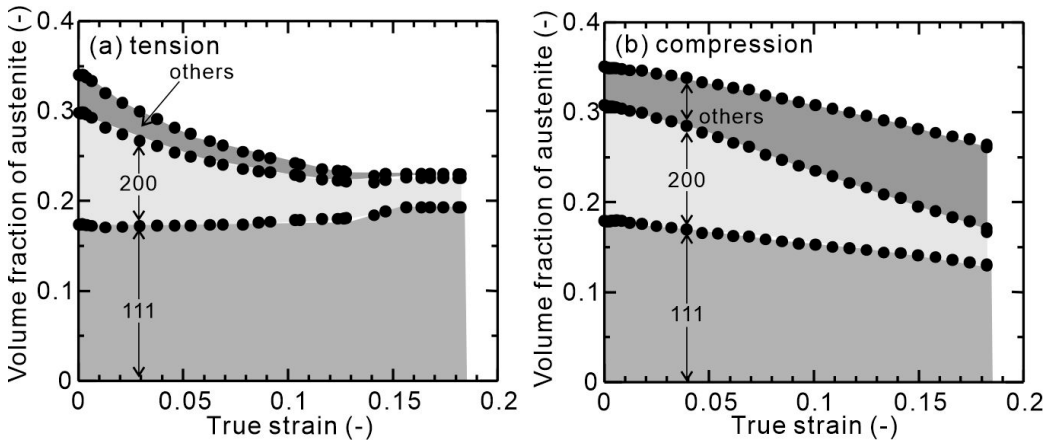

Figure 9. Volume fraction of austenite of the 0.6%C bainitic steel at tension (a) or compression (b). The partial fraction of the austenite whose loading direction was parallel to <111> or <200> was evaluated with the equation (2).

After the yielding, the curves of these lattice strains show no cross point when compared in the same phase, as shown in Fig.6. This indicates that the crystallographic dependence of deformation dispersion is governed mainly by the elastic anisotropy as indicated by eq. (2), even after the macroscopic yielding. The large difference of stress condition at the austenite grains with different crystallographic orientation should be related to the crystallographic dependence of the deformation-induced martensitic transformation, as predicted in the previous paper [3]. However, it should be noted that the relativity of the magnitude of the stress dispersion does not change between the tension and the compression.

The difference in the lattice strain of the FCC phase between the tension and compression is clearly found in the change of the slope at the yielding (Fig.6). All of the increasing rate of the FCC lattice strain at the tension decreases after yielding, while the rate at the compression shows no decreasing. This should be due to the volume expansion in the deformation-induced martensitic transformation. The expansion with the martensitic transformation occurs both at the tension and at the compression, and it partially supports the plastic tensile deformation while it can act as resistance against the compressive deformation.

Volume fraction of retained austenite and texture

As shown in Fig.3, the diffraction measurement system was arranged to fix the diffraction vector parallel to the lording axis. This means that the relative peak intensity at TAKUMI indicates the concentration of corresponding orientation parallel to the loading axis. On the other hand, the diameter of the specimen changes plastically with keeping constant volume. Thus, when the raw intensity was modified for the change of sample diameter as the calculation to obtain true stress and standardized by initial intensity, the modified intensity indicates the concentration of the corresponding orientation parallel to the loading axis.

Figure 8 shows the modified relative intensity of the 0.6%C bainitic steel at the tension (a) and the compression (b). The data were plotted as a function of applied true stress. These intensities started changing significantly when the applied stress reached to the macroscopic yield stress. Concerning of the BCC at the tension, the <110> increased and the <200> decreased. These changes were reversed at the compression. The <211> intensity showed relatively neutral both at the tension and at the compression. On the other hand, this reversal found in the BCC was not observed in the FCC orientations. The relative intensity of <200> and <311> of the FCC decreased both at the tension and compression. Although these changes should imply the effect of the stress polarity on the transformation, the diffraction intensity includes not only the the change of orientation concentration but also the difference of the diffraction scattering factors. Thus, the volume fraction of austenite should be evaluated by the proper method [33].

Figure 9 shows the total volume fraction of the austenite as a function of applied strain. The total volume of austenite at the tension decreases more largely than at the compression. The effect of stress condition on the martensitic transformation has been discussed for long time [30] and the result that the difference in kinematical change of austenite volume fraction at the tension and at the compression found in this work shows consistent with the previous works [26,34]. The difference between the tension and the compression tends to become largely with increasing of the carbon content when this data is compared with the previously reported data shown in Fig.2.

The deformation-induced martensitic transformation occurs with the strong orientation dependence [3,20] under the plastic deformation accompanied with the crystallographic rotation, it should be useful to consider the texture component at the given stress condition. When the applied stress is fixed, the contents of the texture component in the volume fraction of austenite can be estimated with the data obtained at TAKUMI. This is because the diffraction vector was parallel to the loading axis. The fraction of content of the austenite grains with <*hkl*> parallel to the loading direction was calculated by the following equation (2) with the corresponding peak intensity, I^{γ}_{hkl} , and the materials scattering factor, R^{γ}_{hkl} [33], and the volume fraction of austenite, V^{γ}.

$$(content\ of\ the\ austenite\ grains\ with < hkl > parallel\ to\ the\ loading\ axis\ ) = V^{\gamma}\left(\frac{I^{\gamma}_{hkl}R^{\gamma}_{hkl}}{\Sigma_{h'k'h'}I^{\gamma}_{h'k'h'}R^{\gamma}_{h'k'h'}}\right) \quad (2)$$

The content of austenite grains with <111> or <200> parallel to the loading axis were additionally illustrated in Fig. 9. The <111> contents show significantly different tendency from the total volume fraction of austenite: the <111> content increased

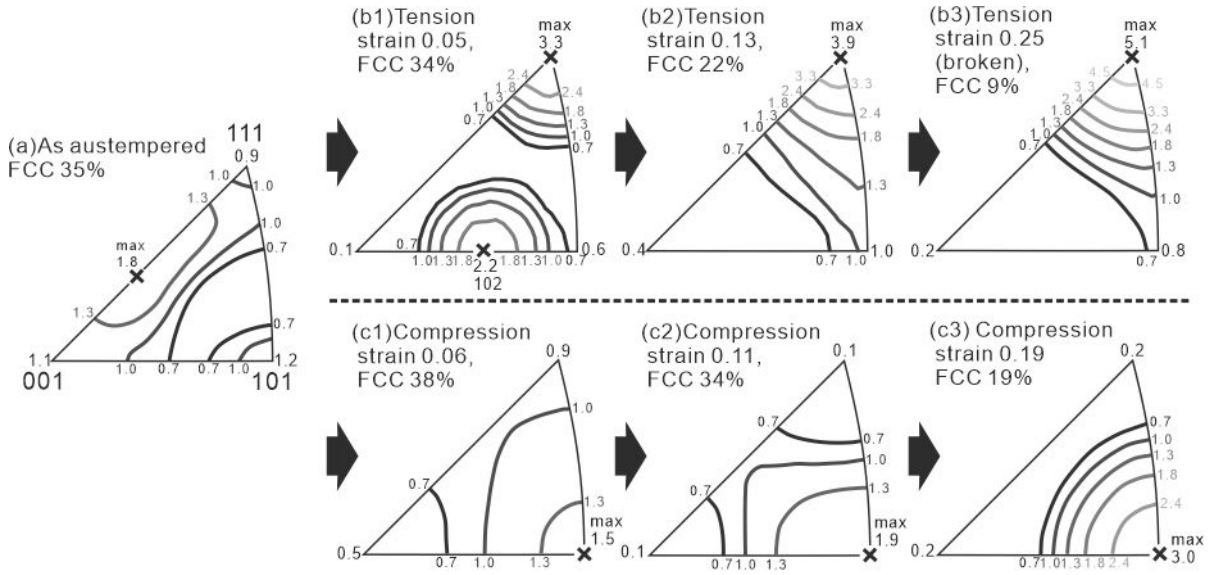

Figure 10. Inverse pole figures of the loading axes of the 0.6%C bainitic steel. (a) as austempered, (b) tension and (c) compression.

slightly at the tension, while it decreased at the compression. On the other hand, both the <200> contents at the tension and at the compression showed similar to those of the total volume fraction of austenite.

There should be two reasons for the change of the texture components of the volume fraction of austenite. One is the evolution of deformation texture and the another is the orientation dependence on the deformation-induced martensitic transformation. **Figure 10** shows the inverse pole figures showing the loading direction of the 0.6%C bainitic steel as austempered (a), at the tension (b), and at the compression (c). These data were obtained by the EBSD measurement with the samples deformed to different strains. Concerning to the deformation texture, the orientation parallel to the hypotenuse orientation (<111> to <001>) tends to remain at the tension; whereas <101> // loading axis is the main component of compressive deformation. According to the orientation dependence on the deformation-induced martensitic transformation, the mechanism proposed by Bogers and Burgers model [35] implied that the slip of the imperfect dislocation whose Burgers vector is parallel to <112> leading partial dislocation in FCC crystal is the primitive control process of the martensitic transformation [36]. Based on this model and the stress partitioning due to the elastic anisotropy, the authors explained the <001> appears the preferable loading axis for the deformation-induced transformation [3]. However, the austenite grains rotate to the different orientation where the loading axis is far from both <001> and <111>. This means that the synergy of both two effects (the deformation texture and the transformation mechanism) should bring the dependence of the stress polarity on the kinetics of deformation-induced phase transformation. The deformation texture changes with the grain size and other microstructural morphology which changes with the total carbon content of the bainitic steel. Thus, the deformation texture should be one of the key points to explain the difference of the stress polarity dependence among the different carbon content.

CONCLUSIONS

Deformation induced martensitic transformation during tensile or compressive deformation of the high-carbon bainitic steel (0.62wt%C-2.02%Si-0.23%Mn-1.01%Cr-Fe) was studied. The microstructure before the deformation was bainite with the retained austenite whose volume fraction was 35%. The tensile deformation is accompanied by more significant work hardening than that at the compression. This was due to the suppression of deformation induced martensitic transformation at the compression, which was confirmed mainly by the in situ neutron diffraction at TAKUMI, J-PARC. It was also found that the increasing lattice strain at austenite by tensile deformation retarded with the deformation-induced martensitic transformation, while this retardation was not found at the compression. The mechanism for the suppression of the deformation-induced martensitic transformation at the compression should be related to (1) the evolution of the deformation texture and (2) the orientation dependence of the martensitic transformation.

ACKNOWLEDGEMENTS

This study is based on work supported by a Grant-in-Aid for Scientific Research (ID: 20H02488) through the Japan Society for the Promotion of Science (JSPS). The neutron diffraction experiments were performed at BL19 in Materials and Life Science Experimental Facility of J-PARC with the proposal of 2021B0371.

REFERENCES

1. V.F. Zackay, E.R. Parker, D. Fahr, R. Bush, "The enhancement of ductility in high-strength steels", *Transaction of American Society of Metals*, 60 (1967), pp.252-259.
2. B.C. De Cooman, "Structure-properties relationship in TRIP steels containing carbide-free bainite", *Current Opinion in Solid State and Materials Science*, 8(2004), pp.285-303.
3. R. Ueji, A. Shibata, K. Ushioda, Y. Kimura, T. Ohmura, T. Inoue, "Crystallographic orientation dependence of deformation-induced martensitic transformation of 1.3 GPa-class 0.6 %C bainitic steel with retained austenite", *Scripta Materialia*, 194(2021), 113666.
4. D.B. Santos, R. Barbosa, P.P. de Oliveier, E.V. Pereloma, ”Mechanical Behavior and Microstructure of High Carbon Si–Mn–Cr Steel with Trip Effect", *ISIJ International*, 49(2009), pp.1592-1600.
5. K. Suzuki, Y. Ono, G. Miyamoto, T. Furuhara, "Microstructure and mechanical properties of austempered medium carbon steels", *Tetsu-to-Hagané*, 97(2011), pp.26-33.
6. C. Garcia-Mateo, F.G. Caballero, T. Sourmail, M. Kuntz, J. Cornide, V. Smanio, R. Elvira, "Tensile behaviour of a nanocrystalline bainitic steel containing 3 wt% silicon", *Materials Science and Engineering A*, 549(2012), pp.185-192.
7. R. Ueji, Y. Kimura, K. Ushioda, T. Ohmura, T. Inoue, "Bainite transformation and resultant tensile properties of 0.6%C low alloyed steels with different austenite grain sizes", *ISIJ International*, 61(2021), pp.582-590.

8. K. Shinoda and T. Yamada, "Mechanical properties of a Si-Mn steel with mixed structure of bainite and retained austenite", *Netsu-Shori (Journal of Japan Society of Heat Treatment)*, 20(1980), pp.326-330.

9. O. Matsumura, Y. Sakuma, H. Takechi, "Enhancement of elongation by retained austenite in intercritical annealed 0.4C-1.5Si-0.8Mn Steel", *Transactions of the Iron and Steel Institute of Japan*, 27(1987), pp.570-579.

10. O. Matsumura, Y. Sakuma, H. Takechi, "TRIP and its kinetics aspects in austempered 0.4C-1.5Si-0.8Mn steel", *Scripta Metallurgica*, 21(1987), pp.1301-1306.

11. Y. Sakuma, O. Matsumura, O. Akine, "Influence of C content and annealing temperature on microstructure and mechanical properties of 400 °C transformed steel containing retained austenite", *ISIJ International*, 31(1991) pp.1348-1353.

12. Y. Sakuma, O. Matsumura, H. Takechi, "Mechanical properties and retained austenite in intercritically heat-treated bainite-transformed steel and their variation with Si and Mn additions", *Metallurgical Transactions A*, 22A(1991), pp.489- 498.

13. S. Zhang, K.O. Findley, "Quantitative assessment of the effects of microstructure on the stability of retained austenite in TRIP steels", *Acta Materialia*, 61(2013), pp.1895-1903.

14. R. Ding, D. Tang, A. Zhao, "A novel design to enhance the amount of retained austenite and mechanical properties in low-alloyed steel", *Scripta Materialia*, 88(2014), pp.21-24.

15. N. Tsuchida, S. Ohkuda, T. Tanaka, Y. Toji, "High-speed tensile deformation behavior of 1 GPa-grade TRIP-aided multi-phase steels", *ISIJ International*, 58(2018), pp.978-986

16. T. Yamashita, N. Koga, O. Umezawa, "Influence of deformability of retained austenite on martensitic transformation in tension for low alloy steel at low temperatures", *ISIJ International*, 58(2018), 1155-1161.

17. K. Sugimoto, M. Tsunezawa, T. Hojo, S. Ikeda, "Ductility of 0.1-0.6C-1.5Si-1.5Mn ultra high-strength TRIP-aided sheet steels with bainitic ferrite matrix", *ISIJ International*, 44(2004), pp.1608-1614.

18. G. Gao, H. Zhang, X. Gui, Z. Tan, B. Bai, Y. Weng, "Enhanced strain hardening capacity in a lean alloy steel treated by a “disturbed” bainitic austempering process", *Acta Materialia*, 101(2015), pp.31-39.

19. H. Matsuda, H. Noro, Y. Nagataki, Y. Hosoya, "Effect of retained austenite stability on mechanical properties of 590MPa grade TRIP sheet steels", *Materials Science Forum*, 638-642(2010), pp.3374-3379.

20. D. De Knijf, T. Nguyen-Minh, R.H. Petrov, L.A.I. Kestens, J.J. Jonas, "Orientation dependence of the martensite transformation in a quenched and partitioned steel subjected to uniaxial tension", *Journal of Applied Crystallography*, 47(2014), pp.1261-1266.

21. N. Tsuchida, Y. Morimoto, T. Tonan, Y. Shibata, K. Fukaura, R. Ueji, "Stress-induced martensitic transformation behaviors at various temperatures and their effects in SUS304 metastable austenitic stainless steel", *ISIJ International*, 51(2011), pp.124-129.

22. Y. Takagi, R. Ueji, T. Mizuguchi, N. Tsuchida, "Influence of strain rate on TRIP effect in SUS301L metastable austenite steel", *Tetsu-to-Hagané*,, 97(2011), pp.450-456.

23. T. Angel, "Formation of martensite in austenitic stainless steels, - effects of deformation, temperature, and composition", *Journal of the Iron and Steel Institute*, 177(1954), pp.165-174.

24. K. Sugimoto, M. Kobayashi, S. Hashimoto, "Ductility and strain-induced transformation in a high-strength transformation induced plasticity-aided dual-phase steel", *Metallurgical transactions A*, 23A(1992) pp.3085-3091.

25. Y.F. Shen, L.N. Qiu, X. Sun, L. Zuo, P.K. Liaw, D. Raabe, "Effects of retained austenite volume fraction, morphology, and carbon content on strength and ductility of nanostructured TRIP-assisted steels", *Materials Science and Engineering A*, 636(2015), pp.551-564.

26. H. Kawata, T. Yasutomi, S. Shirakami, K. Nakamura, E. Sakurada, "Deformation-induced martensite transformation behavior during tensile and compressive deformation in low-alloy TRIP steel sheets", *ISIJ International*, 61(2021), pp.527-536

27. R. Oishi, M. Yonemura, Y. Nishimaki, S. Torii, A. Hoshikawa, T. Ishigaki, T. Morishima, K. Mori, T. Kamiyama, "Rietveld analysis software for J-PARC", *Nuclear Instruments and Methods in Physics Research Section A*, 600(2009), pp.94-96.

28. S. Harjo, N. Tsuchida, J. Abe, W. Gong, "Martensite phase stress and the strengthening mechanism in TRIP steel by neutron diffraction", *Scientific Reports*, 7(2017) 15149.

29. K. Sugimoto, T. Iida, J. Sakaguchi, T. Kashima, "Retained austenite characteristics and tensile properties of a TRIP type bainitic sheet steel", *ISIJ International*, 40(2000), pp.902-908.

30. J.R. Patel, M. Cohen, "Criterion for the action of applied stress in the martensitic transformation", *Acta Metallurgica*, 1(1953), pp.531-538.

31. A.J. Allen, M. Bourke, W.I.F. David, S. Dawes, M.T. Hutchings, A.D. Krawitz, C.G. Windsor, "Effects of elastic anisotropy on the lattice strains in polycrystalline metals and composites measured by neutron diffraction", in: G. Beck, S. Denis, A. Simon (Eds.), *Proceedings of the International Conference on Residual Stresses*, Springer, (1989), pp.78–83.

32. W.F. Hosford, *The Mechanics of Crystals and Textured Polycrystals*, Oxford University Press, (1993), p.19.

33. A.K. De, D.C. Murdock, M.C. Mataya, J.G. Speer, D.K. Matlock, "Quantitative measurement of deformation-induced martensite in 304 stainless steel by X-ray diffraction", *Scripta Materialia*, 50(2004), pp.1445-1449.

34. A.M. Beese, D. Mohr, "Effect of stress triaxiality and Lode angle on the kinetics of strain-induced austenite-to-martensite transformation", *Acta Materialia*, 59(2011), pp.2589-2600.

35. A.J. Bogers, W.G. Burgers, "Partial dislocations on the {110} planes in the B.C.C. lattice and the transition of the F.C.C. into the B.C.C. lattice", *Acta Metallurgica*. 12 (1964), pp.255–260.

36. M. Kato, T. Mori, "Stress-induced martensite in single crystals of an Fe-23Ni-5Cr alloy", *Acta Metallurgica*, 24(1976), pp.853-860.

